Natale *et al. Alzheimer's Research & Therapy* (2026) 18:116
https://doi.org/10.1186/s13195-026-02014-7

Alzheimer's Research & Therapy

RESEARCH Open Access

Intranasal administration of neural stem cell-derived extracellular vesicles prevents cognitive decline in both male and female 3×Tg-AD mice by dampening neuroinflammation and epigenetically regulating amyloid β metabolism

Francesca Natale[1,2†], Alice Dellaria[1†], Ida Nifo Sarrapochiello[1], Lucia Leone[1,2], Matteo Spinelli[1,3], Marco Rinaudo[1,2], Nicoletta Garofalo[1], Claudio Grassi[1,2*] and Salvatore Fusco[1,2]

Abstract

Background Alzheimer's disease (AD) is the leading cause of dementia in the elderly and poses a significant socioeconomic burden due to its progressive nature and lack of effective treatments. Recent studies suggest that neural stem cell-derived extracellular vesicles (NSC-EV) hold therapeutic potential against AD by delivering bioactive molecules that counteract neuroinflammation, oxidative stress, and protein dysregulation.

Methods NSC-EV were intranasally administered to both male and female 3×Tg-AD mice from three to twelve months of age and cognitive function were evaluated at multiple time points. Moreover, neuroinflammation and amyloid-β (Aβ) metabolism markers were studied at 9 months of age.

Results Intranasal administration of NSC-EV delayed cognitive decline, reduced hippocampal neuroinflammation, and decreased Aβ accumulation in both male and female 3×Tg-AD mice. These functional effects were accompanied by the downregulation of STAT5 expression, which is a mediator of neuroinflammatory signaling, and the upregulation of neuroprotective transcription factor NRF2. Moreover, the changes in STAT5 and NRF2 expression caused the epigenetic inhibition of pro-amyloidogenic beta secretase BACE1 transcription and the enhanced expression of IDE, which is the main enzyme involved in Aβ clearance. These events were accompanied by the reduction of Aβ levels.

Conclusions Our findings provide new insights into the molecular mechanisms by which NSC-EV modulate AD pathology and support their potential as a regenerative therapy for neurodegenerative diseases.

[†]Francesca Natale and Alice Dellaria contributed equally to this work.

*Correspondence:
Claudio Grassi
claudio.grassi@unicatt.it

Full list of author information is available at the end of the article

Keywords Extracellular vesicles, Neural stem cells, Alzheimer's disease, Neuroinflammation, amyloid-β, Epigenetics, BACE1, Insulin-degrading enzyme

Background

Alzheimer's disease (AD) is a neurodegenerative disorder characterized by multifactorial pathogenesis, ultimately leading to progressive neurodegeneration and cognitive decline [1]. AD has emerged as the leading cause of dementia affecting between 60 and 80% of the world's elderly population [2]. This highlights the strong impact of the disease on global health and the growing need for effective treatment.

Over the years, much effort has been made to understand the pathology of AD and develop therapeutic tools. It is now widely accepted that AD is characterized by the accumulation of amyloid-beta (Aβ) oligomers and the formation of neurofibrillary tangles (NFTs), which are neuropathological hallmarks also used as biomarkers or tracers in neuroimaging techniques [3–5]. Nevertheless, AD has long eluded multiple therapeutic strategies [6].

In recent years, much attention has been paid to the impact of inflammatory processes on AD pathogenesis and progression [7]. Under physiological conditions glial cells, such as astrocytes and microglia, play a key role in the maintenance of brain health and homeostasis, but excess stimulation may cause an increase in proinflammatory cytokine release and aberrant activation of immunomodulatory pathways that produce synaptotoxic effects and neuronal damage [8, 9]. Interestingly, inflammatory cytokines have been shown to regulate the enzymatic activity of beta-secretase 1 (BACE1), an enzyme involved in the synthesis of Aβ peptides [10]. Elevated BACE1 activity leads to increased generation of synaptotoxic Aβ peptides inside the brain [11, 12]. These findings suggest that inflammation is not merely a consequence of AD but an active contributor to its progression.

One promising area of research in this regard is stem cell (SC)-based therapy, which explores the potential of SC and their secretome to counteract the neuroinflammatory environment in neurodegenerative disorders [13]. Extracellular vesicles (EV) are small membrane-bound particles secreted by all cells that carry a variety of biological molecules modulating the physiology of target cells. SC-derived EV have been reported to exhibit regenerative and anti-inflammatory properties, making them an attractive option for treating AD [14].

Recent studies have demonstrated that the SC secretome modulates inflammatory responses, influence metabolic pathways, and counteract cell death, all of which are crucial aspects of AD progression [15]. Moreover, several reports have shown that mesenchymal stromal cell-derived EV inhibit neuroinflammation and exert beneficial effects in experimental AD models [16, 17]. However, the molecular mechanisms underlying the ability of SC-derived EV to prevent AD pathogenesis remain elusive. In our study, we found that intranasal administration of neural stem cell (NSC)-derived EV (NSC-EV) counteracted the onset and progression of cognitive deficits in both male and female 3×Tg-AD mice. NSC-EV reduced Aβ deposition and the activation of both microglia and astrocytes in the hippocampus. Moreover, EV treatment modulated the activation of inflammation- and oxidative stress-related transcription factors, STAT5 and NRF2. Finally, NSC-EV epigenetically regulated the expression of BACE1 and insulin-degrading enzyme (IDE), which are key elements involved in the generation and clearance of Aβ. Our findings reveal an epigenetic mechanism linking STAT5/NRF2 activation, BACE1/IDE expression, and Aβ accumulation, and provide novel insights into the beneficial effects of SC-derived EV on AD onset and progression.

Methods

Animals and treatments

Male and female 3×Tg-AD mice (B6;129-Tg(APPSwe, tauP301L)1Lfa Psen1tm1Mpm/Mmjax) were derived from the Animal facility of Università Cattolica del Sacro Cuore. Mice were housed in groups (3–5 animals per cage) under a 12 h light-dark cycle at constant temperature (22–23 °C), with food and water ad libitum. All experiments were designed according to the ARRIVE guidelines. Mice derived from the same litter were randomly assigned to the following experimental groups. For experiments, 3×Tg-AD mice were intranasally injected with (i) NSC-EV (approximately 1×10^8 diluted in 4μL PBS 1X per each administration) or (ii) saline starting at 3- and continuing until 9- months of age, twice a week. EV treatment started at 3 months of age because at this stage neither male nor female 3×Tg-AD mice still showed any cognitive impairment. The number of vesicles was selected according to our previous studies [18, 19].

NSC culture and EV isolation

NSCs were isolated from both major adult neurogenic niches (i.e., hippocampus and subventricular zone) of P0 C57Bl6 mice. NSCs were expanded and cultured in serum-free NeurobasalA medium supplemented with B27 (minus vitamin A), EGF, and bFGF, under standardized neurosphere conditions as previously described [18]. EVs were isolated exclusively from conditioned media derived from neurosphere cultures, and EV harvesting was restricted to early passages (up to passage 3).

For EV isolation, the media from different primary cultures of murine NSC were collected and pre-cleared using a multistep centrifugation protocol. EV were purified using the exoEasy Maxi Kit (Qiagen) according to the manufacturer's instructions. Isolated EV were subjected to phosphate-buffered saline (PBS) buffer exchange using Vivaspin 2 columns (Sartorius, Goettingen, Germany, cat number VS0232) for in vivo treatment. EV were analyzed and quantified performing Nanoparticle Tracking analysis using a Nanosight NS300 particle size analyser (Malvern Panalytical, UK). Once isolated, the EV were stored at -80 °C.

Behavioural tests

All behavioural tests were performed as previously described [20]. Long-term recognition memory and short-term spatial memory were assessed using Novel Object Recognition (NOR) and Object Place Recognition (OPR) tests, respectively. In the NOR test, on the first day (habituation), animals familiarized for 10 min with the test arena (45 cm×45 cm). On the second day (training session), mice were allowed to explore two identical objects placed symmetrically at the center of the arena for 10 min. On the last day (test session), a new object replaced one of the old objects, and the animals were allowed to explore for 10 min. For the OPR test, animals underwent the same procedure used for the NOR test, except that, during the test phase, one of the objects was moved into a different position without being substituted. In the OPR test, different cues were placed on the walls of the testing arena to provide spatial points of reference. Mice showing a total exploration time lower than 20 s or spending significantly different time between the two objects during the training phase were excluded.

Tests were video-recorded, and the analysis was performed by a blinded experimenter. For both tests, a preference index was calculated in the test phase as the ratio between the time spent exploring the novel object and the total time of object exploration to quantify recognition and spatial memory.

Western blot

Samples for western blot analyses were processed as previously described [21]. Briefly, whole hippocampi were lysed in ice-cold lysis buffer (NaCl 150 mM, Tris-HCL 50mM pH8, EDTA 2mM) containing 1% Triton X-100, 0.5% SDS, 1X protease inhibitor cocktail, 1 mM sodium orthovanadate, 1 mM sodium fluoride and 1 mM phenylmethyl sulfonyl fluoride (all reagents from Sigma Aldrich, St. Louis MO, USA). The lysate was sonicated with a Diagenode Bioruptor Standard water bath sonicator and incubated 15 min on ice. At the end of the incubation, samples were spun down at 13,000 g at 4 °C for 15 min. The supernatant was quantified for protein content using Bradford assay (DC Protein Assay; Bio-Rad, Hercules, CA, USA). Equal amounts of proteins were diluted in 6× Laemmli Buffer, boiled, and resolved using sodium dodecyl-sulfate polyacrylamide gel electrophoresis (SDS-PAGE, Biorad, Hercules, CA, USA). Primary antibodies (listed in Table S1) were diluted 1:1000 in 3% milk in TBS-Tween20, incubated overnight and then revealed with horse radish peroxidase-conjugated secondary antibodies (1:5000 Cell Signaling Technology Inc. Danvers, MA, USA) and different chemiluminescent substrates, according to the expected protein concentration (Cyanagen, BO, Italy).

Signals were acquired on a UVItec Cambridge Alliance instrument and quantified with Alliance Software. The expression levels of the target protein were normalized to the total amount of housekeeping protein (HSP90, β-actin or β-tubulin). The phosphorylation levels of the target proteins were normalized to the total amount of the target protein in each lane and to the total amount of housekeeping protein according to the following formula (phospho-protein/total protein/housekeeping protein). In bar graphs, where relative units were used to show the data, the mean value of the control was set to 1. Representative images of western blot were cropped for presentation with no manipulations. Uncropped blot images are provided in Supplementary Fig. 4.

Immunofluorescence experiments

For immunofluorescence ex vivo experiments, female 3×Tg-AD mice were used because they show higher levels of Aβ deposition at 9 months of age at level of subiculum compared to male mice [22, 23]. The animals were deeply anesthetized and transcardially perfused with PBS (0.1 M pH 7.4), followed by 4% paraformaldehyde (PFA). Once perfusion was completed, the brains were collected, incubated overnight at 4 °C in 4% PFA, and then transferred to a solution of 30% sucrose in H_2O. Brains were then cut into slices (40 µm thick) with a vibratome (VT 100 S, Leica Microsystem, Gmbh, Wetzar, Germany). Immunofluorescence experiments were performed as previously described [20]. Briefly, after 1 h of incubation with blocking buffer made by 0,3% Triton X-100 (Sigma St Louis, MO, USA) and 5% NGS (Euroclone s.p.a., Milan, Italy), tissues were incubated overnight in blocking buffer at 4 °C with primary unconjugated antibodies (GFAP, IBA-1, Aβ, MAP2, all diluted 1:400). The next day, the tissues were incubated for 90 min at RT with secondary antibodies diluted in PBS 1X: Alexa Fluor 546 (TRITC) or Alexa Fluor 488 (FITC) anti-rabbit/mouse according to the primary antibody host species (1:800, Invitrogen, Carlsbad, CA, USA). Finally, the nuclei were counterstained with DAPI (0.5 µg/mL; Invitrogen, Carlsbad, CA, USA) for 10 min, and the slices were coverslipped with Pro-Long Gold anti-fade reagent (Invitrogen, Carlsbad, CA, USA).

Confocal image acquisition and analysis

Images (1024 × 1024 pixels) were acquired using a Nikon A1 MP confocal system (Tokyo, Japan) at 4× and 60× magnifications with a non–oil-immersion objective (NA 1.2). The scale bar is shown in the picture and described in the figure legends. Image analysis was conducted using NIS-Elements AR software version 5.30.01. For ex vivo immunofluorescence analyses, $DAPI^+/IBA\text{-}1^+$ and $DAPI^+/GFAP^+$ co-immunoreactive cells were counted individually in the entire hippocampus of mice. Since GFAP and Amyloid-β are differentially expressed in various conditions and cell types, their levels of expression vary depending on the specific context. Therefore, analyses were performed by comparing immunofluorescence intensities in areas of the same extent (fluorescence intensity measurement/ROI area) between two or more experimental conditions. For biodistribution experiments, image analysis was conducted focusing on $MAP2^+/Exo\text{-}Glow^+$ or $IBA\text{-}1^+/Exo\text{-}Glow^+$ cells. For 3D analyses, the "Slices View" feature of the Nikon NIS Elements Software has been used. Briefly, after a z-stack acquisition of a target image (or ROI) of interest, this view displays orthogonal XY, XZ, and YZ projections of the image sequence and the actual colocalization of signals on the same Z slice. For each immunofluorescence experiment, each experimental group was composed of four animals. For each brain, five slices containing the hippocampus were analyzed. The entire analysis was performed using ImageJ/FIJI software.

ELISA assay

Aβ peptide 1–42 levels were analyzed on whole hippocampi using an Ultrasensitive Human Amyloid beta42 ELISA Kit (Thermo Fisher Scientific). Assays were performed according to the manufacturer's instructions. Aβ1–42 levels are indicated as pg of Aβ peptide 1–42 per milligram of proteins contained in the total lysate.

Multiplex

Cytokine analysis was performed using Q-Plex Mouse HS ArrayTM Technology (Quansys Bio, Logan, Utah, USA). Q-Plex is an ELISA assay intended for simultaneous and quantitative measurements of multiple cytokines in a single sample: GM-CSF (Lower Limit of Quantification – LLOQ: 0.61 pg/mL), IFNγ (LLOQ: 0.54 pg/mL), IL-1α (LLOQ: 0.72 pg/mL), IL-1β (LLOQ: 2.51 pg/mL), IL-2 (LLOQ: 0.38 pg/mL), IL-3 (LLOQ: 0.08 pg/mL), IL-4 (LLOQ: 0.43 pg/mL), IL-5 (LLOQ: 0.54 pg/mL), IL-6 (LLOQ: 0.68 pg/mL), IL-10 (LLOQ: 0.70 pg/mL), IL-12p70 (LLOQ: 0.65 pg/mL), IL-17 (LLOQ: 0.77 pg/mL), MIP-1α (LLOQ: 1.16 pg/mL), RANTES (LLOQ: 2.46 pg/mL), and TNFα (LLOQ: 0.67 pg/mL).Whole hippocampi were lysed and the assay was performed according to the manufacturer's instructions. Briefly, samples were pipetted into the wells of a 96-well plate with immobilized analyte-specific antibodies. After washing, a biotinylated analyte-specific antibody was added. After washing, streptavidin-horseradish peroxidase was. added to the wells and incubated according to the manufacturer's instructions. The amount of conjugated enzyme in each well was measured by adding a chemiluminescent substrate and reading the results using Q-View Software.

ChIP

ChIP assays were performed as previously described [24]. Hippocampi were resuspended in 200 µL lysis buffer containing 1% SDS, 50 mM Tris-HCl pH 8.0, and 10 mM EDTA and sonicated on ice with six 10-s pulses with a 20-s interpulse interval. Approximately 2 µg of specific antibody or control IgG was added overnight at 4 °C. Chromatin fragments were extracted with a PCR DNA fragment purification kit (Geneaid). The primers used for promoter analysis are listed in Table S2.

Real-time PCR

Quantitative real-time PCR was carried out using Power SYBRR Master Mix (Fisher Molecular Biology) on AB7500 instrument (Life Technologies) according to the manufacturer's instructions. The thermal cycling profile included a pre-incubation step of 94 °C for 10 min, followed by 40 cycles of denaturation (94 °C, 15 s), annealing (60 °C, 30 s), and elongation (72 °C, 20 s). Then, melting curves were generated by heating amplified products at 94 °C for 15 s, cooling to 50 °C for 30 s, followed by slow heating to 94 °C in increments of 0.5 °C and they confirmed that only single products had been amplified. ROX was used in the SYBR master mix as reference dye and all data were analyzed by comparing to the amplification levels of the Actin. The threshold values determined by the software were used to calculate gene expression levels employing the cycle-at-threshold (Ct) method. The data are expressed as fold changes (compared to control) for each target, using the 2-ΔΔCt approach. The primer list is shown in Table S3.

Statistical analysis

Sample sizes ($n = 12$ for behavioral tests; $n = 5$ for immunofluorescence experiments; $n = 6$ for multiplex and ELISA assays, western blotting and ChIP analyses) were chosen with adequate power (0.8) according to the results of prior pilot datasets or studies, including our own, that used similar methods or paradigms. Sample estimation and statistical analyses were performed using SigmaPlot 14 software. The statistical tests employed in the experiments (i.e., Student's t-test, two-way ANOVA without or with multiple comparisons) are mentioned in the corresponding figure legend. The level of significance was set at $p < 0.05$. The results are shown as mean ± SEM.

Results

Intranasal administration of NSC-EV prevents memory deficits in 3×Tg-AD mice

To evaluate the efficacy of NSC-EV on the onset and progression of cognitive deficits, we isolated EV from in vitro NSC cultures as previously described [19] (Supplementary Figs. 1A, B) and intranasally treated both male and female 3×Tg-AD mice with vehicle solution (PBS) or NSC-EV starting from 3 months of age. Labeled EV were detected inside both neurons and microglia in the hippocampus 24 h after the intranasal administration (Supplementary Figs. 1 C, D). We tested the cognitive performance of mice using novel object recognition (NOR) and object place recognition (OPR) tasks after 3 or 6 months from the beginning of the treatment (Fig. 1A). Administration of NSC-EV ameliorated the preference index (PI) in males at each age but no significant differences were detectable before 9 months of age (PI in NOR: $F_{2,92}$ = 11.24, 67.3 ± 1.8% for 3×Tg-AD_{NSC-EV} vs. 61.0 ± 1.6% for 3×Tg-AD_{VEH} and P = 0.074 at 6 months, 65.3 ± 1.8% for 3×Tg-AD_{NSC-EV} vs. 58.4 ± 1.6% 3xTg-AD_{VEH} and P = 0.011 at 9 months; PI in OPR: $F_{2,92}$ = 10.93, 64.5 ± 1.1% for 3×Tg-AD_{NSC-EV} vs. 60.7 ± 1.7% for 3×Tg-AD_{VEH} and P = 0.291 at 6 months, 64.2 ± 2.1% for 3×Tg-AD_{NSC-EV} vs. 58.1 ± 2.3% for 3×Tg-AD_{VEH} and P = 0.003 at 9 months; Fig. 1B).

Moreover, the beneficial effects of NSC-EV in both hippocampus-dependent tests were even more evident in female 3×Tg-AD mice at each stage (PI in NOR: $F_{2,92}$ = 29.68, 65.2 ± 3.1% for 3×Tg-AD_{NSC-EV} vs. 56.2 ± 1.8% for 3×Tg-AD_{VEH} and P = 0.0027 at 6 months, 62.6 ± 1.1% for 3×Tg-AD_{NSC-EV} vs. 54.6 ± 1.8% 3xTg-AD_{VEH} and P = 0.0005 at 9 months; PI in OPR: $F_{2,92}$ = 20.21, 64,9 ± 3.9% for 3×Tg-AD_{NSC-EV} vs. 56.0 ± 3.2% for 3×Tg-AD_{VEH} and P = 0.0244 at 6 months, 62.6 ± 3.7% for 3×Tg-AD_{NSC-EV} vs. 54.9 ± 2.1% for 3×Tg-AD_{VEH} and P = 0.0036 at 9 months; Fig. 1C).

NSC-EV reduced neuroinflammation in the hippocampus of 3×Tg-AD mice

To evaluate the effects of EV treatment on AD-related neuroinflammation, we investigated immunoreactivity for ionized calcium-binding adaptor molecule 1 (IBA1), a marker of microglial activation, and glial fibrillary acidic protein (GFAP), a well-established cytoskeletal marker of astrogliosis, in the hippocampus of 3×Tg-AD mice. Immunofluorescence analyses revealed a reduction of IBA1 immunopositive cell number upon NSC-EV administration in both female and male mice ($IBA1^+$ cell number: $F_{3,49}$ = 47.206, 315.4 ± 16.3 vs. 437.4 ± 41.1, P = 0.0192 for females; 127.4 ± 17.9 vs. 230.9 ± 20.9, P = 0.0036 for males; Figs. 2A, B, E). Similar effects were observed for GFAP immunoreactivity in the hippocampus of 3×Tg-AD_{NSC-EV} mice (GFAP fluorescence intensity: $F_{3,49}$ = 7.795, -29.6% and P = 0.0036 for females; -23.8% and P = 0.0418 for males; Figs. 2C, D, F). Accordingly, analysis of either immunoreactivity or expression of CD68, which is a highly selective marker for monocytes and macrophages, also showed a significant reduction in the hippocampi of 3×Tg-AD mice after NSC-EV treatment ($CD68^+$ cell number: 20.6 ± 1.4 vs. 57.8 ± 8.3, P = 0.0023; CD68 expression: -60%, P = 0.0056; Supplementary Figs. 2A, B). We also analyzed the levels of both proinflammatory and anti-inflammatory cytokines in the hippocampal tissue. We found decreased levels of several proinflammatory cytokines in 3×Tg-AD_{NSC-EV} (GM-CSF – 67%, P = 0.011; IFNɣ -59% P = 0.028; IL-1α -178% P = 0.0004; IL-1β -53% P = 0.032; IL-10 -59%, P = 0.04; IL-17 -64%, P = 0.018; MIP-1α -200%, P = 0.027; RANTES – 58%, P = 0.020; TNFα -54%, P = 0.030; Fig. 2G). No changes were detected in the levels of other cytokines, including anti-inflammatory ones (IL-3, IL-4, IL-5, and IL-6; Fig. 2G).

NSC-EV influenced the expression of enzymes regulating Aβ metabolism

First, we assessed Aβ levels in the hippocampus of 3×Tg-AD_{VEH} and 3×Tg-AD_{NSC-EV} mice. Immunofluorescence analysis revealed a decrease in hippocampal Aβ deposition upon NSC-EV administration in 9-month-old female mice (-35.5%, P = 0.027; Fig. 3A).

Moreover, we found reduced levels of Aβ1–42 in the hippocampus of both male and female 3×Tg-AD animals treated with NSC-EV (males: 168.8 ± 17.9 for 3×Tg-AD_{NSC-EV} vs. 216.3 ± 12.9 for 3×Tg-AD_{VEH}, P = 0.0403; females: 2979.9 ± 412.4 for 3×Tg-AD_{NSC-EV} vs. 4614.9 ± 560.6 for 3×Tg-AD_{VEH}, P = 0.0273; Fig. 3B) as measured by ELISA. Based on these results, we wondered whether the reduction in hippocampal Aβ load was driven by altered expression or activity of enzymes involved in Aβ metabolism. Immunoblot analysis revealed changes in the expression of key proteins regulating Aβ genesis and clearance. In particular, we observed a significant decrease in BACE1 and an enhancement of IDE expression in the hippocampus of 3×Tg-AD mice upon NSC-EV administration (BACE1 -34%, P = 0.037; IDE + 49%, P = 0.006; Fig. 3C). No significant changes in both APP and Tau phosphorylation, and Neprilysin expression were detected (Fig. 3C). Accordingly, NSC-EV treatment did not alter the activation levels of GSK3β, which is the main kinase regulating Tau phosphorylation (Fig. 3C).

NSC-EV epigenetically regulated BACE1 and IDE expression by modulating transcription factors STAT5 and NRF2

Several inflammation- and oxidative stress-related transcription factors have been reported to regulate the expression of BACE1 in the brain [25, 26]. We analysed the levels of a set of transcription factors (i.e., STAT5,

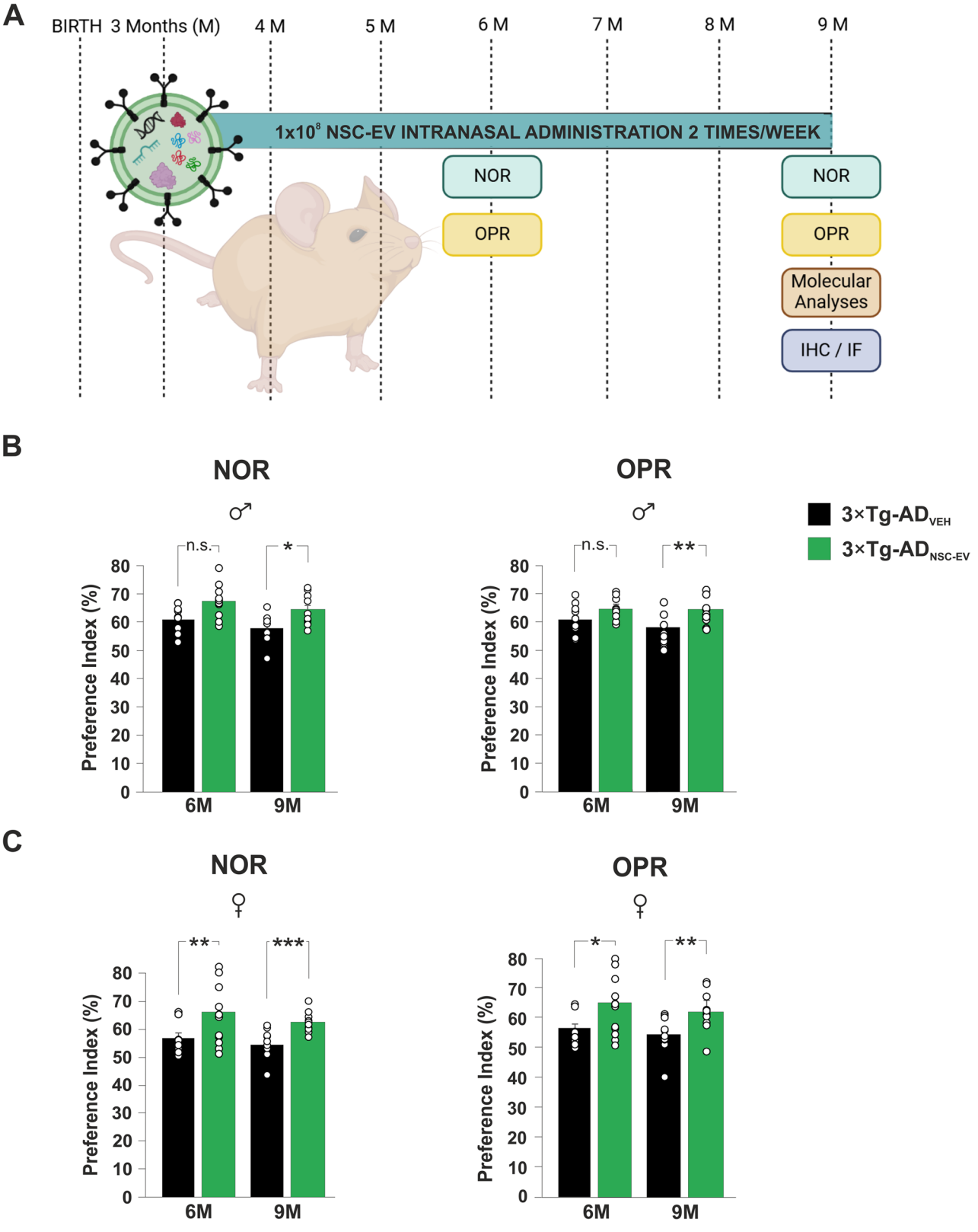

Fig. 1 NSC-EV counteracted the onset and progression of memory deficits in 3×Tg-AD mice. **A** Schematic representation of 3×Tg-AD mice treatment and timeline of experimental procedures (NOR; OPR; IHC, immunohistochemistry; IF, immunofluorescence). Bar graphs showing preference indices of 6- and 9-month-old (**B**) male and (**C**) female 3×Tg-AD mice in NOR (left) and OPR (right) behavioral tests ($n = 10–11$ males and 9–12 females per group; statistics by repeated measures ANOVA and Sidak's multiple comparisons post-hoc test). Data are expressed as mean ± SEM. *$P < 0.05$; **$P < 0.01$; ***$P < 0.001$; n.s. not significant

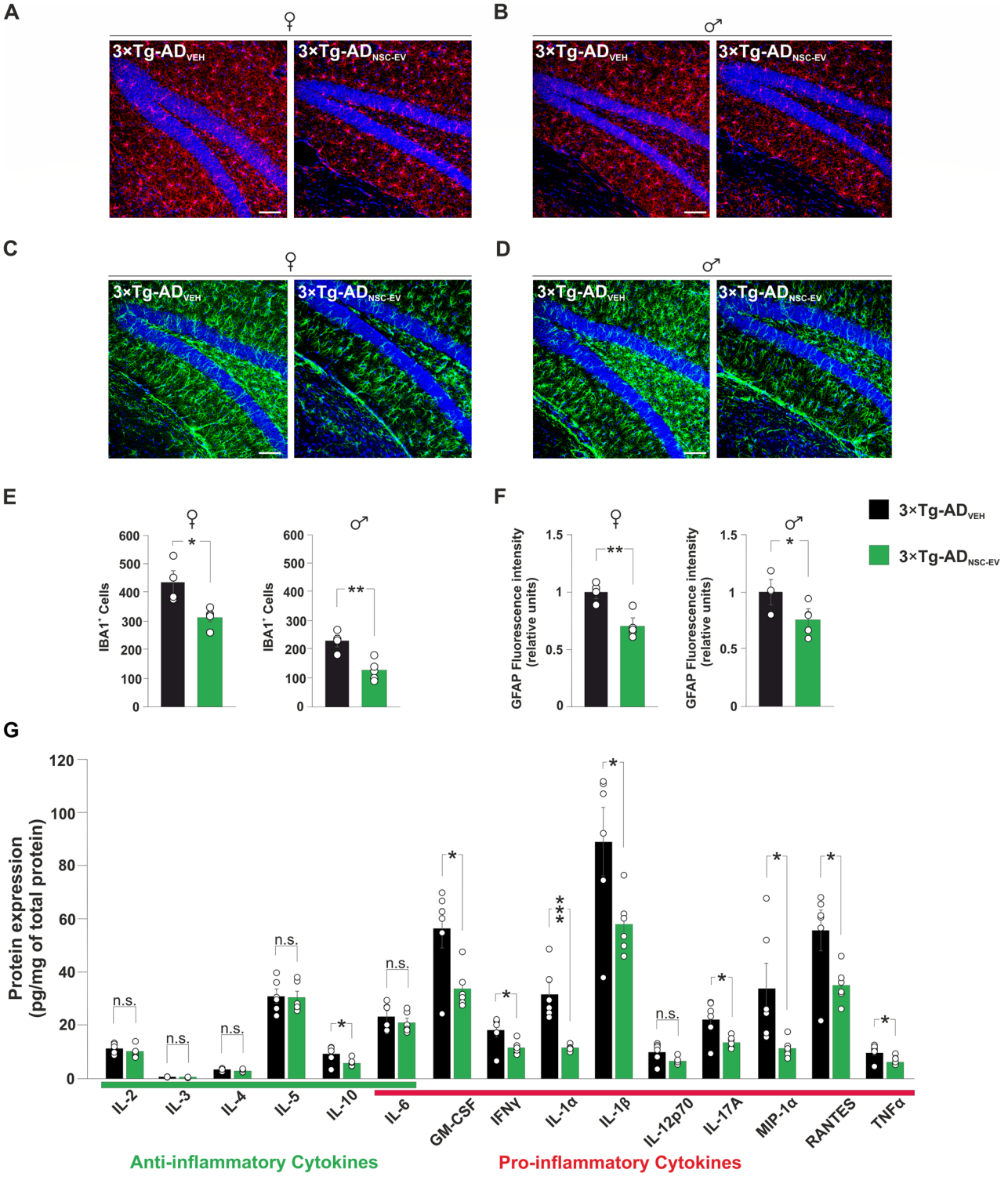

Fig. 2 Intranasal administration of NSC-EV inhibited neuroinflammation in 3×Tg-AD hippocampal tissues. Representative immunostaining of (**A**, **B**) IBA1 (red) and (**C**, **D**) GFAP (green) in the hippocampus of female and male 3×Tg-AD$_{VEH}$ and 3×Tg-AD$_{NSC-EV}$ animals. Scale bar: 50 µm. Bar graphs showing (**E**) IBA1 and (**F**) GFAP immunoreactivity in the hippocampus of female (left) and male (right) 3×Tg-AD$_{VEH}$ and 3×Tg-AD$_{NSC-EV}$ animals ($n = 4$–5 mice per group, 5 brain slices were analyzed for each animal; statistics by two-way ANOVA and Bonferroni post-hoc tests). **G** Bar graphs showing the levels of IL-2, IL-3, IL-4, IL-5, IL-10, IL-6, GM-CSF, IFNγ, IL-1α, IL-1β, IL-12p70, IL-17 A, MIP-1α, RANTES, and TNFα in hippocampal tissues of 3×Tg-AD$_{VEH}$ and 3×Tg-AD$_{NSC-EV}$ mice ($n = 6$ female mice per group; statistics by unpaired Student's *t*-test). Multiplex analyses were performed in triplicate. Data are expressed as mean ± SEM. *$P < 0.05$; **$P < 0.01$; ***$P < 0.001$; n.s. not significant

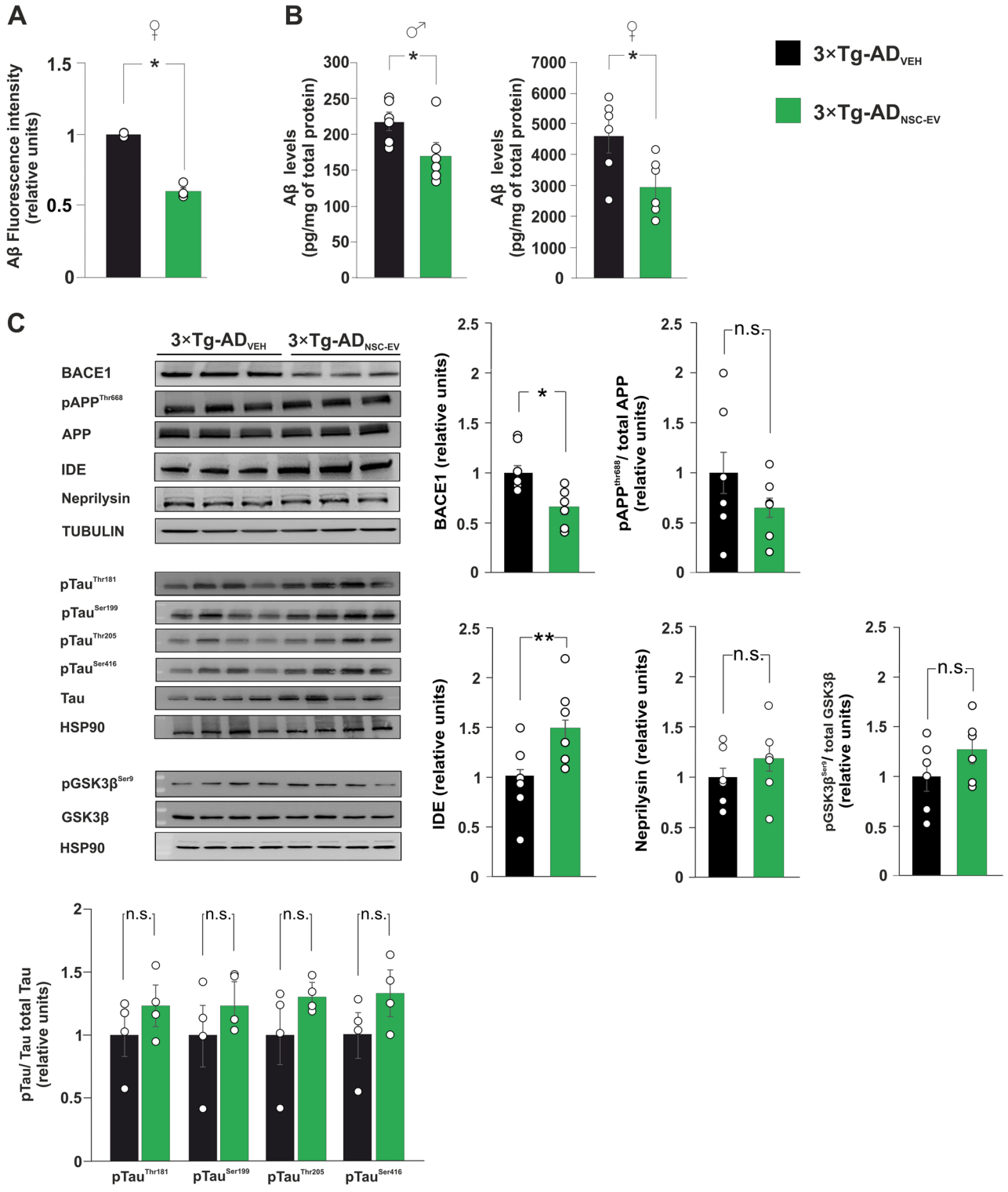

Fig. 3 NSC-EV decreased Aβ peptide levels in the hippocampus of 3×Tg-AD mice by modulating the expression of BACE1 and IDE. **A** Bar graph showing fluorescence intensity of immunoreactive Aβ peptides and oligomers in hippocampal tissue of 3×Tg-AD$_{VEH}$ and 3×Tg-AD$_{NSC-EV}$ mice ($n = 4$ female mice per each group, 5 brain slices have been analyzed for each animal; statistics by unpaired Student's *t*-test). **B** Bar graphs showing the levels of Aβ1–42 peptide in the hippocampus of male (left) and female (right) 3×Tg-AD$_{VEH}$ and 3×Tg-AD$_{NSC-EV}$ mice. ELISA assays were performed in triplicate ($n = 6$ mice per group; statistical analysis using unpaired Student's *t*-test). **C** Representative immunoblots (left) and bar graphs (right and bottom) showing the expression of BACE1, IDE and Neprilysin and the phosphorylation levels of APP and Tau in the hippocampus of 3×Tg-AD$_{VEH}$ and 3×Tg-AD$_{NSC-EV}$ mice ($n = 6$ mice for each group composed of males and females; statistics by unpaired Student's *t*-test). Data are expressed as mean ± SEM. $^{*}P < 0.05$; $^{**}P < 0.01$; n.s. not significant

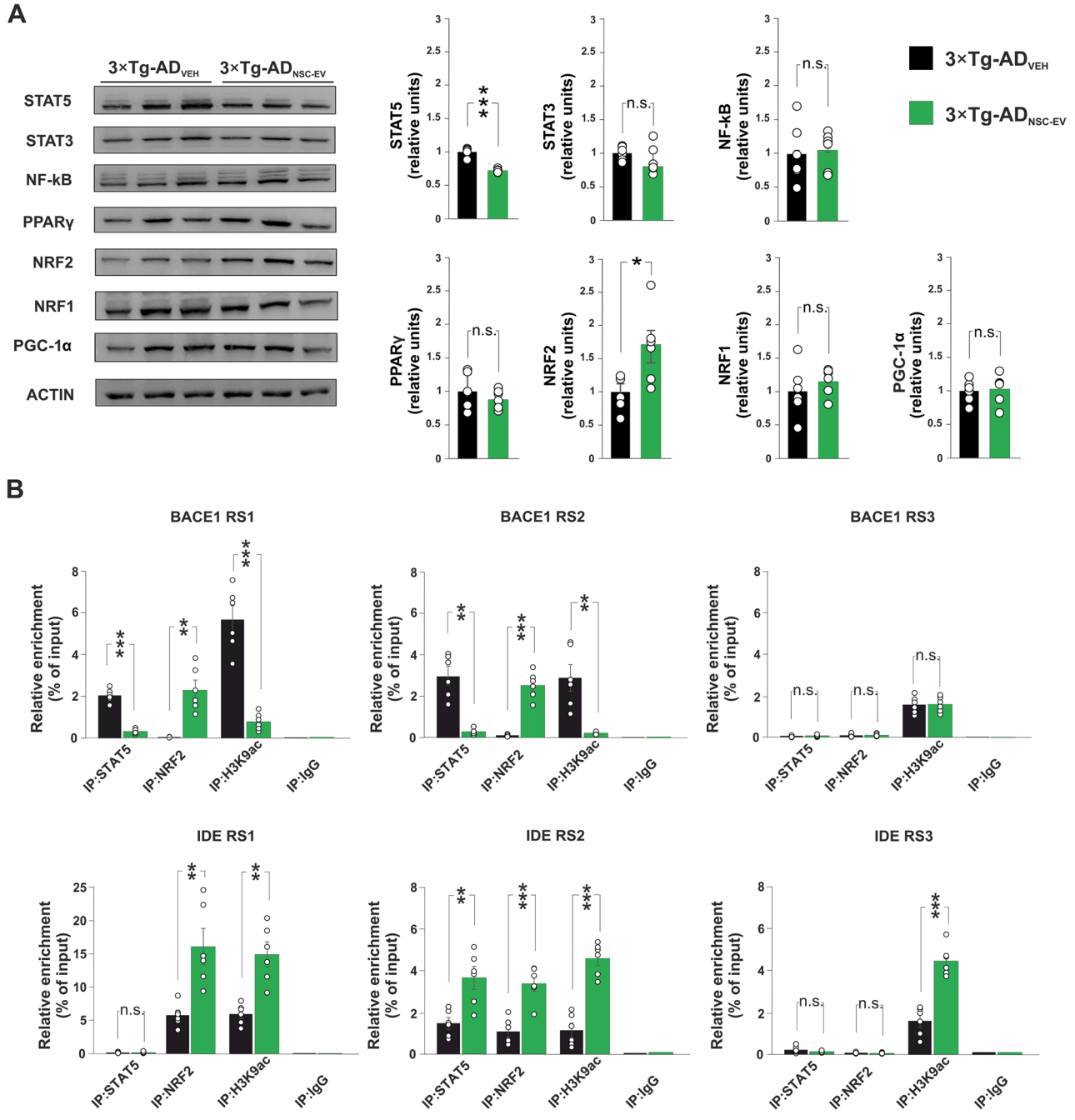

Fig. 4 NSC-EV epigenetically regulated BACE1 and IDE through the transcription factors STAT5 and NRF2. **A** Representative immunoblots (left) and bar graphs (right) showing the expression levels of the transcriptional factors STAT5, STAT3, NF-kB, PPARγ, NRF1, NRF2, and PGC-1α in the hippocampus of 3×Tg-AD$_{VEH}$ and 3×Tg-AD$_{NSC-EV}$ mice ($n = 6$ mice per group, comprising males and females; statistics by unpaired Student's *t*-test). **B** ChIP assays showing the binding of STAT5, NRF2, and histone 3 lysine 9 acetylation (H3K9ac) on the selected regulatory sequences (RS) of BACE1 (upper panel) and IDE (bottom panel) genes in the hippocampus of 3×Tg-AD$_{VEH}$ and 3×Tg-AD$_{NSC-EV}$ mice ($n = 6$ mice per group composed of males and females; statistics by two-way ANOVA and Bonferroni post-hoc test). Data are expressed as mean ± SEM. *$P < 0.05$; **$P < 0.01$; ***$P < 0.001$; n.s. not significant

STAT3, NF-kB, PPARγ, NRF1, NRF2, and PGC-1α) that are regulated by neuroinflammatory signals and may trigger AD-related neurodegeneration. Immunoblot analysis of hippocampal lysates showed lower levels of STAT5 and increased NRF2 expression in 3×Tg-AD mice after NSC-EV treatment (STAT5: -29%, $P = 1.18 \times 10^{-6}$; NRF2: +71%, $P = 0.016$; Fig. 4A). Conversely, the expression of STAT3, NF-kB, PPARγ, NRF1, and PGC-1α did not significantly change compared to the controls (Fig. 4A).

To investigate a potential link among neuroinflammation inhibition, altered expression of the transcription factors STAT5 and NRF2, and changes of BACE1

and IDE levels, we analyzed the regulatory sequences of BACE1 and IDE genes. Bioinformatic analysis of the mouse BACE1 (NC_000075.7) and IDE (NC_000085.7) loci revealed the presence of several putative antioxidant- or STAT-responsive elements (ARE or SRE, respectively) upstream of the starting codon of both genes (BACE1 regulatory sequences, RS: RS1 -941, RS2 -1261, RS3 -2175; IDE RS: RS1 -138, RS2 -577, RS3 -1762). Chromatin immunoprecipitation (ChIP) experiments performed on hippocampal lysates showed that both STAT5 and NRF2 were able to bind several sequences on BACE1 and IDE promoters. Moreover, NSC-EV administration differentially modulated the recruitment of transcription factors and epigenetic activation of the same regulatory sequences. In particular, NSC-EV reduced the binding of STAT5 and increased the recruitment of NRF2 on BACE1 promoter regions (BACE1 RS1: $F_{2.603}$ = 41.189; STAT5 -85.3% and $P = 1.43 \times 10^{-5}$, NRF2, +9600% and $P = 0.00313$; BACE1 RS2: $F_{2.603}$ = 22.642; STAT5 -90% and $P = 0.00143$, NRF2 + 2238% and $P = 0.00026$; Fig. 4B). In addition, lysine 9 acetylation of histone 3 (H3K9ac) on the same regulatory sequences was significantly reduced in 3×Tg-AD_{NSC-EV} mice (BACE1 RS1: $F_{2.603}$ = 41.189, -86.5% and $P = 0.00025$; BACE1 RS2: $F_{2.603}$ = 22.642, -86.5% and $P = 0.00609$; Fig. 4B). NSC-EV treatment also altered the binding of both STAT5 and NRF2, and modified the epigenetic marker H3K9ac on the promoters of IDE (IDE RS1: $F_{2.603}$ = 30.299; NRF2 + 280% and $P = 0.00683$, H3K9ac + 250% and $P = 0.00274$; IDE RS2: $F_{2.603}$ = 22.316; STAT5 + 247% and $P = 0.00608$, NRF2 + 310% and $P = 0.00041$; H3K9ac + 405% and $P = 1.38 \times 10^{-5}$; IDE RS3: $F_{2.603}$ = 99.899; H3K9ac + 282% and $P = 3.24 \times 10^{-5}$; Fig. 4B). We also investigated the expression of some NRF2 targets in the hippocampus of 3×Tg-AD mice and we found elevated levels of both Heme oxigenase-1 (HO1) and Glutamate-Cysteine Ligase Catalytic subunit (GCLC) upon NSC-EV treatment (HO1, + 93.5% and $p = 0.0098$; GCLC, + 109.9% and $p = 0.0171$; Supplementary Fig. 4A). Finally, ChIP assays showed elevated levels of both NRF2 binding and H3K9 acetylation on the promoters of HO1 and GCLC genes in the hippocampus of 3×Tg-AD_{NSC-EV} mice (HO1 promoter: $F_{3.287}$ = 31.275, NRF2 + 1366% and $P = 0.00061$, H3K9ac + 966% and $P = 0.00129$;.GCLC promoter: $F_{3.287}$ = 73.814, NRF2 + 320% and $P = 0.00219$, H3K9ac + 673% and $P = 8.94 \times 10^{-5}$; Supplementary Fig. 4B).

Discussion

AD is the primary cause of dementia in the elderly population [27, 28]. The progressively more disabling course of the pathology, the impact of the disease on the lives of both patients and their families, and the lack of effective treatments make AD one of the most serious threats to the health system from a socio-economic perspective [29]. Recently, SC-derived EV have been proposed as a new tool against the progression of neurodegenerative disease-related brain function impairment and cognitive decline [30, 31]. Indeed, SC-derived EV cargo contains a plethora of bioactive molecules exerting immunomodulatory and neurotrophic activity and potentially counteracting age- and neuroinflammation-dependent brain disorders [32]. We previously demonstrated that intranasal administration of NSC-EV delivered EV into the hippocampus and prevented brain insulin resistance-related cognitive decline in experimental models of metabolic diseases [18, 19]. Considering the common molecular determinants underlying the impact of metabolic disorders and AD on brain function, which include neuroinflammation, oxidative stress, alteration of brain insulin signaling, and protein homeostasis [33–35], we decided to test the same therapeutic approach in an experimental model of AD. We found that NSC-EV treatment delayed the onset and slowed the progression of cognitive deficits in both male and female 3×Tg-AD mice (Fig. 1). NSC-EV administration also dampened the neuroinflammatory environment and reduced Aβ deposition in the hippocampus of both sexes (Figs. 2 and 3A and B). To date, the accumulation of Aβ oligomers and hyperphosphorylation of Tau remain the two primary pathological hallmarks of AD [36, 37]. SC-derived EV have been reported to reduce Aβ accumulation and protect against Aβ42-induced neuronal toxicity in AD experimental models [38, 39]. However, the molecular mechanisms underlying the effects of EV on Aβ-related neurodegeneration are still poorly understood. We analysed the expression of the main enzymes involved in Aβ metabolism and found a reduction in BACE1 and an increase in IDE levels in the hippocampus of 3×Tg-AD mice after NSC-EV administration (Fig. 3C). Conversely, no alterations of Tau phosphorylation were detectable upon NSC-EV administration. Several studies showed that some therapeutic approaches may efficiently reduce Aβ load without affecting Tau hyper-phosphorylation and vice versa [40–42]. Interestingly, it has been reported that intravenous administration of mesenchymal stem cells reduces Tau phosphorylation in 3×Tg-AD mice without altering Aβ levels [43], suggesting that stem cell-derived secretome may differentially impact on either Aβ or Tau pathways. Accordingly, the phosphorylation levels of GSK3β were not significantly changed upon NSC-EV treatment. BACE1 is an amyloid precursor protein-cleaving enzyme that plays a crucial role in the generation of neurotoxic Aβ [44]. Expectedly, BACE1 is a key drug target for slowing Aβ production in early AD [45, 46]. IDE is a protease that plays a pivotal role in the degradation of Aβ oligomers at the cell surface and in the extracellular space [47]. It is also involved in insulin clearance and has been proposed as a molecular link between metabolic disease and

AD pathophysiology [48–50]. Several inflammation- and oxidative stress-responsive transcription factors have been implicated in the regulation of both BACE1 and IDE genes [51–53]. Thus, we tested the hypothesis that NSC-EV ameliorated the AD phenotype in 3×Tg-AD mice by modulating the activity of transcriptional regulators of BACE1 and IDE expression. Immunoblot analysis revealed a reduction in STAT5 expression and higher levels of NRF2 in the hippocampus of 3×Tg-AD_{NSC-EV} mice (Fig. 4A). Signaling through the JAK2-STAT5 pathway has been reported to play a crucial role in cytokine-induced microglial activation [54]. In addition, upregulation of STAT5 has been associated with experimental models of AD [55]. Moreover, NRF2 has been described as a promising therapeutic target for AD because of its ability to counteract neurodegeneration by stimulating antioxidative defense, improving mitochondrial function, promoting proteostasis, and inhibiting neuroinflammation [56, 57]. Alterations in epigenetic mechanisms regulating transcription have been widely accepted as key mechanisms underlying the onset and progression of neurodegeneration [58–61]. After NSC-EV treatment, we observed changes in the H3K9ac epigenetic marker on the regulatory sequences of BACE1 and IDE genes that were coherent with the alteration of their expression levels (Fig. 4B). The recruitment of both NRF2 and STAT5 to the promoters of the same genes was in line with the modification of expression levels observed for both transcription factors (Fig. 4B). We also found epigenetic activation and higher expression of NRF2 target genes in the hippocampus of 3×Tg-AD mice after NSC-EV treatment (Supplementary Fig. 4). Accordingly, NRF2 has been reported to negatively regulate BACE1 expression in human and mouse AD experimental models, whereas it enhances the transcriptional expression of IDE in the liver [62, 63]. Moreover, JAK/STAT transcription factors have been demonstrated to promote the transcription of BACE1 in response to neuroinflammatory stimuli [64, 65]. Microglial and astrocytic activation play central roles in sustaining the neuroinflammatory milieu in AD [66, 67]. Our data indicate that intranasal administration of NSC-EV reduced both hippocampal neuroinflammation and Aβ accumulation and ameliorated the AD phenotype in 3×Tg-AD mice by modulating the STAT5- and NRF2-mediated epigenetic regulation of BACE1 and IDE expression. However, the molecular players in the NSC-EV cargo responsible for their therapeutic effects remain unclear. miRNome analysis performed on the cargo of EV derived from human NSC revealed promising candidates targeting neuroinflammation and synaptic function, such as miR-124-3p, miR-125b-5p, and miR-125a-5p [68]. Accordingly, several miRNAs have been characterized for their post-transcriptional regulation of NRF2 and IDE [69, 70]. We previously reported higher levels of the neurotrophic factor BDNF in NSC-EV [19]. Moreover, NSC-EV have been shown to reduce apoptosis and neuroinflammation by activating autophagy in the central nervous system [71].

Limitations

The exact impact of each bioactive molecule in the milieu of NSC-EV cargo is difficult to delineate, considering the heterogeneous effects of SC-derived EV on multiple pathways and the potential synergistic effects of the combined action of different molecules on several targets [32, 72].

Conclusions

Our findings highlight a novel mechanism underlying the impact of NSC-EV on Aβ deposition, neurodegeneration, and cognitive decline. Regenerative medicine has emerged as a potential field offering innovative and adjuvant therapeutic tools for neurological disorders, and SC-derived EV represent the most promising and translational avenue. Recently, fibroblast-derived induced NSC have been reported to ameliorate the AD phenotype in 5×FAD mice [73]. Ongoing and future studies are necessary to unveil their usefulness and efficacy on AD patients.

Abbreviations

AD	Alzheimer's Disease
APP	Amyloid Precursor Protein
Aβ	Amyloid-beta
BACE-1	Beta-site Amyloid Precursor Protein Cleaving Enzyme 1
EV	Extracellular Vesicles
IDE	Insulin-Degrading Enzyme
IL	Interleukin
NF-κB	Nuclear Factor kappa-light-chain-enhancer of activated B cells
NFTs	Neurofibrillary Tangles
NSC-EV	Neural stem cell-derived extracellular vesicles
NSC	Neural Stem Cells
SC-EV	Stem cell-derived extracellular vesicles
TNF	Tumor Necrosis Factor

Supplementary Information

The online version contains supplementary material available at https://doi.org/10.1186/s13195-026-02014-7.

Supplementary Material 1.

Supplementary Material 2.

Acknowledgements

This research was supported by Ministero della Salute-Ricerca Corrente 2026. Figure 1A was created using BioRender.com (2025). We would like to acknowledge the contribution of the Microscopy Core Facilities Gemelli Science and Technology Park of Fondazione Policlinico Universitario "A. Gemelli" IRCCS.

Authors' contributions

Conceptualization: F.N., S.F. and C.G.; methodology: F.N., I.N.S. and M.S.; validation: F.N. and M.R.; formal analysis: F.N., A.D. and S.F.; investigation: F.N., A.D., I.N.S., L.L, M.S., M.R., and N.G.; visualization: A.D.; writing – original draft: F.N. and A.D.; writing – review and editing: S.F. and C.G.; supervision: S.F. and

C.G.; Project administration: S.F.; funding acquisition: C.G and. S.F. All authors read and approved the final manuscript.

Funding
None.

Data availability
The datasets supporting the conclusions of this article are included within the article and its additional files.

Declarations

Ethics approval and consent to participate
All procedures performed on animals were approved by the Ethics Committee of Università Cattolica del Sacro Cuore (authorization no. 949/2023-PR) in accordance with the Italian (Ministry of Health guideline, Legislative Decree No 116/1992) and European Union legislation governing animal research (Directive 2010/63/EU). Consent to Participate and Consent to Publish declarations: not applicable.

Consent for publication
Not applicable.

Competing interests
The authors declare no competing interests.

Author details
[1]Department of Neuroscience, Università Cattolica del Sacro Cuore, Rome 00168, Italy
[2]Fondazione Policlinico Universitario A. Gemelli IRCCS, Rome 00168, Italy
[3]Present address: Department of Biomedical Sciences, University of Sassari, Sassari 07100, Italy

Received: 21 October 2025 / Accepted: 11 March 2026
Published online: 01 April 2026

References

1. Boyd RJ, Avramopoulos D, Jantzie LL, McCallion AS. Neuroinflammation represents a common theme amongst genetic and environmental risk factors for Alzheimer and Parkinson diseases. J Neuroinflammation. 2022;19(1):223. https://doi.org/10.1186/s12974-022-02584-x.
2. Li X, Feng X, Sun X, Hou N, Han F, Liu Y. Global, regional, and national burden of Alzheimer's disease and other dementias, 1990–2019. Front Aging Neurosci. 2022;14:937486. https://doi.org/10.3389/fnagi.2022.937486.
3. Zhang H, Wei W, Zhao M, Ma L, Jiang X, Pei H, Cao Y, Li H. Interaction between Aβ and Tau in the Pathogenesis of Alzheimer's Disease. Int J Biol Sci. 2021;17:2181–9.
4. Hodson R. Alzheimer's disease. Nature. 2018;559(S1). https://doi.org/10.1038/d41586-018-05717-6.
5. Kamatham PT, Shukla R, Khatri DK, Vora LK. Pathogenesis, diagnostics, and therapeutics for Alzheimer's disease: Breaking the memory barrier. Ageing Res Rev. 2024;101:102481. https://doi.org/10.1016/j.arr.2024.102481.
6. Makin S. The future of Alzheimer's treatment. Nature. 2025;640:S4–6.
7. Yiannopoulou KG, Papageorgiou SG. Current and Future Treatments in Alzheimer Disease: An Update. J Cent Nerv Syst Disease. 2020;12:1179573520907397. https://doi.org/10.1177/1179573520907397.
8. Javanmehr N, Saleki K, Alijanizadeh P, Rezaei N. Microglia dynamics in aging-related neurobehavioral and neuroinflammatory diseases. J Neuroinflammation. 2002;19(1):273. https://doi.org/10.1186/s12974-022-02637-1.
9. Morales I, Guzman-Martinez L, Cerda-Troncoso C, Farias GA, Maccioni RB. Neuroinflammation in the pathogenesis of Alzheimer's disease. A rational framework for the search of novel therapeutic approaches. Front Cell Neurosci. 2014;8:112.
10. Calsolaro V, Edison P. Neuroinflammation in Alzheimer's disease: Current evidence and future directions. Alzheimers Dement. 2016;12(6):719–32. https://doi.org/10.1016/j.jalz.2016.02.010.
11. Hampel H, Vassar R, De Strooper B, et al. The β-Secretase BACE1 in Alzheimer's Disease. Biol Psychiatry. 2021;89(8):745–56. https://doi.org/10.1016/j.biopsych.2020.02.001.
12. Coimbra JRM, Resende R, Custódio JBA, Salvador JAR, Santos AE. BACE1 Inhibitors for Alzheimer's Disease: Current Challenges and Future Perspectives. J Alzheimers Dis. 2024;101(s1):S53–78. https://doi.org/10.3233/JAD-240146.
13. Palanisamy CP, et al. New strategies of neurodegenerative disease treatment with extracellular vesicles (EVs) derived from mesenchymal stem cells (MSCs). Theranostics. 2023;13(12):4138–65. https://doi.org/10.7150/thno.83066.
14. Moghassemi S, Dadashzadeh A, Sousa MJ, Vlieghe H, Yang J, León-Félix CM, Amorim CA. Extracellular vesicles in nanomedicine and regenerative medicine: A review over the last decade. Bioactive Mater. 2024;36:126–56. https://doi.org/10.1016/j.bioactmat.2024.02.021.
15. Da Silva K, et al. The paradigm of stem cell secretome in tissue repair and regeneration: Present and future perspectives. Wound Repair Regeneration. 2025;33(1):e13251. https://doi.org/10.1111/wrr.13251.
16. Cone AS, et al. Mesenchymal stem cell-derived extracellular vesicles ameliorate Alzheimer's disease-like phenotypes in a preclinical mouse model. Theranostics. 2021;11(17):8129–42. https://doi.org/10.7150/thno.62069.
17. Losurdo M, Pedrazzoli M, D'Agostino C, Elia CA, Massenzio F, Lonati E, et al. Intranasal delivery of mesenchymal stem cell-derived extracellular vesicles exerts immunomodulatory and neuroprotective effects in a 3xTg model of Alzheimer's disease. Stem Cells Translational Med. 2020;9(9):1068–84. https://doi.org/10.1002/sctm.19-0327.
18. Natale F, Leone L, Rinaudo M, Sollazzo R, Barbati SA, La Greca F, et al. Neural Stem Cell-Derived Extracellular Vesicles Counteract Insulin Resistance-Induced Senescence of Neurogenic Niche. Stem Cells. 2022;40(3):318–31. https://doi.org/10.1093/stmcls/sxab026.
19. Spinelli M, Natale F, Rinaudo M, Leone L, Mezzogori D, Fusco S, Grassi C. Neural Stem Cell-Derived Exosomes Revert HFD-Dependent Memory Impairment via CREB-BDNF Signalling. Int J Mol Sci. 2020;21(23):8994. https://doi.org/10.3390/ijms21238994.
20. Natale F, Spinelli M, Rinaudo M, Gulisano W, Nifo Sarrapochiello I, Aceto G, et al. Inhibition of zDHHC7-driven protein S-palmitoylation prevents cognitive deficits in an experimental model of Alzheimer's disease. Proc Natl Acad Sci USA. 2024;121(49):e2402604121. https://doi.org/10.1073/pnas.2402604121.
21. Zuliani I, Lanzillotta C, Tramutola A, Barone E, Perluigi M, Rinaldo S, et al. High-Fat Diet Leads to Reduced Protein O-GlcNAcylation and Mitochondrial Defects Promoting the Development of Alzheimer's Disease Signatures. Int J Mol Sci. 2021;22(7):3746. https://doi.org/10.3390/ijms22073746.
22. Hu YT, Chen XL, Zhang YN, McGurran H, Stormmesand J, Breeuwsma N, Sluiter A, Zhao J, Swaab D, Bao AM. Sex differences in hippocampal β-amyloid accumulation in the triple-transgenic mouse model of Alzheimer's disease and the potential role of local estrogens. Front Neurosci. 2023;17:1117584. https://doi.org/10.3389/fnins.2023.1117584.
23. Carroll JC, Rosario ER, Kreimer S, Villamagna A, Gentzschein E, Stanczyk FZ, Pike CJ. Sex differences in β-amyloid accumulation in 3xTg-AD mice: role of neonatal sex steroid hormone exposure. Brain Res. 2010;1366:233–45. https://doi.org/10.1016/j.brainres.2010.10.009.
24. Ripoli C, Spinelli M, Natale F, Fusco S, Grassi C. Glucose Overload Inhibits Glutamatergic Synaptic Transmission: A Novel Role for CREB-Mediated Regulation of Synaptotagmins 2 and 4. Front Cell Dev Biology. 2020;8:810. https://doi.org/10.3389/fcell.2020.00810.
25. Rossner S, Sastre M, Bourne K, Lichtenthaler SF. Transcriptional and translational regulation of BACE1 expression–implications for Alzheimer's disease. Prog Neurobiol. 2006;79(2):95–111. https://doi.org/10.1016/j.pneurobio.2006.06.001.
26. Kwak YD, Wang R, Li JJ, Zhang YW, Xu H, Liao FF. Differential regulation of BACE1 expression by oxidative and nitrosative signals. Mol Neurodegeneration. 2011;6:17. https://doi.org/10.1186/1750-1326-6-17.
27. Scheltens P, Blennow K, Breteler MM, de Strooper B, Frisoni GB, Salloway S, Van der Flier WM. Alzheimer's disease. Lancet. 2016;388(10043):505–17. https://doi.org/10.1016/S0140-6736(15)01124-1.
28. Serrano-Pozo A, Das S, Hyman BT. APOE and Alzheimer's disease: advances in genetics, pathophysiology, and therapeutic approaches. Lancet Neurol. 2021;20(1):68–80. https://doi.org/10.1016/S1474-4422(20)30412-9.
29. Angrist M, Yang A, Kantor B, Chiba-Falek O. Good problems to have? Policy and societal implications of a disease-modifying therapy for presymptomatic late-onset Alzheimer's disease. Life Sci Soc Policy. 2020;16(1):11. https://doi.org/10.1186/s40504-020-00106-2.
30. Natale F, Fusco S, Grassi C. Dual role of brain-derived extracellular vesicles in dementia-related neurodegenerative disorders: cargo of disease spreading signals and diagnostic-therapeutic molecules. Translational Neurodegeneration. 2022;11(1):50. https://doi.org/10.1186/s40035-022-00326-w.

31. Kaur M, Fusco S, Van den Broek B, Aseervatham J, Rostami A, Iacovitti L, et al. Most recent advances and applications of extracellular vesicles in tackling neurological challenges. Med Res Rev. 2024;44(4):1923–66. https://doi.org/10.1002/med.22035.
32. Spinelli M, Fusco S, Grassi C. Therapeutic potential of stem cell-derived extracellular vesicles in neurodegenerative diseases associated with cognitive decline. Stem Cells. 2025;43(2):sxae074. https://doi.org/10.1093/stmcls/sxae074.
33. Lemche E, Killick R, Mitchell J, Caton PW, Choudhary P, Howard JK. Molecular mechanisms linking type 2 diabetes mellitus and late-onset Alzheimer's disease: A systematic review and qualitative meta-analysis. Neurobiol Dis. 2024;196:106485. https://doi.org/10.1016/j.nbd.2024.106485.
34. Spinelli M, Fusco S, Grassi C. Brain insulin resistance impairs hippocampal plasticity. Vitamins Horm. 2020;114:281–306. https://doi.org/10.1016/bs.vh.2020.04.005.
35. Yang LG, March ZM, Stephenson RA, Narayan PS. Apolipoprotein E in lipid metabolism and neurodegenerative disease. Trends Endocrinol Metabolism. 2023;34(8):430–45. https://doi.org/10.1016/j.tem.2023.05.002.
36. Sengupta U, Kayed R. Amyloid β, Tau, and α-Synuclein aggregates in the pathogenesis, prognosis, and therapeutics for neurodegenerative diseases. Prog Neurobiol. 2022;214:102270. https://doi.org/10.1016/j.pneurobio.2022.102270.
37. Wu M, Zhang M, Yin X, Chen K, Hu Z, Zhou Q, et al. The role of pathological tau in synaptic dysfunction in Alzheimer's diseases. Translational Neurodegeneration. 2021;10(1):45. https://doi.org/10.1186/s40035-021-00270-1.
38. Liew LC, Katsuda T, Gailhouste L, Nakagama H, Ochiya T. Mesenchymal stem cell-derived extracellular vesicles: a glimmer of hope in treating Alzheimer's disease. Int Immunol. 2017;29(1):11–9. https://doi.org/10.1093/intimm/dxx002.
39. Rao S, Madhu LN, Babu RS, Shankar G, Kotian S, Nagarajan A, et al. Extracellular vesicles from hiPSC-derived NSCs protect human neurons against Aβ-42 oligomers induced neurodegeneration, mitochondrial dysfunction and tau phosphorylation. Stem Cell Res Ther. 2025;16(1):191. https://doi.org/10.1186/s13287-025-04324-3.
40. Oddo S, Billings L, Kesslak JP, Cribbs DH, LaFerla FM. Abeta immunotherapy leads to clearance of early, but not late, hyperphosphorylated tau aggregates via the proteasome. Neuron. 2004;43(3):321–32. https://doi.org/10.1016/j.neuron.2004.07.003.
41. Parachikova A, Vasilevko V, Cribbs DH, LaFerla FM, Green KN. Reductions in amyloid-beta-derived neuroinflammation, with minocycline, restore cognition but do not significantly affect tau hyperphosphorylation. J Alzheimers Dis. 2010;21(2):527–42. https://doi.org/10.3233/JAD-2010-100204.
42. Caccamo A, Oddo S, Tran LX, LaFerla FM. Lithium reduces tau phosphorylation but not A beta or working memory deficits in a transgenic model with both plaques and tangles. Am J Pathol. 2007;170(5):1669–75. https://doi.org/10.2353/ajpath.2007.061178.
43. Neves AF, Camargo C, Premer C, Hare JM, Baumel BS, Pinto M. Intravenous administration of mesenchymal stem cells reduces Tau phosphorylation and inflammation in the 3xTg-AD mouse model of Alzheimer's disease. Exp Neurol. 2021;341:113706. https://doi.org/10.1016/j.expneurol.2021.113706.
44. Lombardo S, Chiacchiaretta M, Tarr A, Kim W, Cao T, Sigal G, et al. BACE1 partial deletion induces synaptic plasticity deficit in adult mice. Sci Rep. 2019;9:19877.
45. Wessels AM, Tariot PN, Zimmer JA, Selzler KJ, Bragg SM, Andersen SW, et al. Efficacy and safety of lanabecestat for treatment of early and mild Alzheimer disease: The AMARANTH and DAYBREAK-ALZ randomized clinical trials. JAMA Neurol. 2020;77:199–209.
46. Hampel H, Vassar R, De Strooper B, Hardy J, Willem M, Singh N, et al. The β-Secretase BACE1 in Alzheimer's Disease. Biol Psychiatry. 2021;89(8):745–56. https://doi.org/10.1016/j.biopsych.2020.02.001.
47. Thakur S, Dhapola R, Sarma P, Medhi B, Reddy DH. Neuroinflammation in Alzheimer's Disease: Current Progress in Molecular Signaling and Therapeutics. Inflammation. 2023;46(1):1–17. https://doi.org/10.1007/s10753-022-01721-1.
48. Mittal K, Katare DP. Shared links between type 2 diabetes mellitus and Alzheimer's disease: a review. Diabetes Metabolic Syndrome. 2016. https://doi.org/10.1016/j.dsx.2016.01.021.
49. Sposato V, Canu N, Fico E, Fusco S, Bolasco G, Ciotti MT, et al. The Medial Septum Is Insulin Resistant in the AD Presymptomatic Phase: Rescue by Nerve Growth Factor-Driven IRS1 Activation. Mol Neurobiol. 2019;56(1):535–52. https://doi.org/10.1007/s12035-018-1038-4.
50. Qiu WQ, Folstein MF. Insulin, insulin-degrading enzyme and amyloid-beta peptide in Alzheimer's disease: review and hypothesis. Neurobiol Aging. 2006;27(2):190–8.
51. Rossner S, Sastre M, Bourne K, Lichtenthaler SF Transcriptional and translational regulation of BACE1 expression--implications for Alzheimer's disease. Prog Neurobiol. 2006;79(2):95–111. . https://doi.org/10.1016/j.pneurobio.2006.06.001.
52. Natale F, Spinelli M, Rinaudo M, Cocco S, Nifo Sarrapochiello I, Fusco S, Grassi C. Maternal High Fat Diet Anticipates the AD-like Phenotype in 3xTg-AD Mice by Epigenetic Dysregulation of Aβ Metabolism. Cells. 2023;12(2):220. https://doi.org/10.3390/cells12020220.
53. Zhang L, Ding Q, Wang Z. Nuclear respiratory factor 1 mediates the transcription initiation of insulin-degrading enzyme in a TATA box-binding protein-independent manner. PLoS ONE. 2012;7(8):e42035. https://doi.org/10.1371/journal.pone.0042035.
54. Natarajan C, Sriram S, Muthian G, Bright JJ. Signaling through JAK2-STAT5 pathway is essential for IL-3-induced activation of microglia. Glia. 2004;45(2):188–96. https://doi.org/10.1002/glia.10316.
55. Ball BK, Kuhn MK, Bechtel F, Proctor RM, E. A., Brubaker DK. Metabolites associated with type 2 diabetes and Alzheimer's disease trigger differential intracellular signaling responses in mouse primary neurons. Brain Res. 2025;1864:149819. https://doi.org/10.1016/j.brainres.2025.149819.
56. Qu Z, Sun J, Zhang W, Yu J, Zhuang C. Transcription factor NRF2 as a promising therapeutic target for Alzheimer's disease. Free Radic Biol Med. 2020;159:87–102. https://doi.org/10.1016/j.freeradbiomed.2020.06.028.
57. Saha S, Buttari B, Profumo E, Tucci P, Saso L. A Perspective on Nrf2 Signaling Pathway for Neuroinflammation: A Potential Therapeutic Target in Alzheimer's and Parkinson's Diseases. Front Cell Neurosci. 2022;15:787258. https://doi.org/10.3389/fncel.2021.787258.
58. Wang L, Shui X, Diao Y, Chen D, Zhou Y, Lee TH. Potential Implications of miRNAs in the Pathogenesis, Diagnosis, and Therapeutics of Alzheimer's Disease. Int J Mol Sci. 2023;24(22):16259. https://doi.org/10.3390/ijms242216259.
59. Marmolejo-Garza A, Medeiros-Furquim T, Rao R, Eggen BJL, Boddeke E, Dolga AM. Transcriptomic and epigenomic landscapes of Alzheimer's disease evidence mitochondrial-related pathways. Biochim et Biophys Acta - Mol Cell Res. 2022;1869(10):119326. https://doi.org/10.1016/j.bbamcr.2022.119326.
60. Men J, Wang X, Zhou Y, Huang Y, Zheng Y, Wang Y, et al. Neurodegenerative diseases: Epigenetic regulatory mechanisms and therapeutic potential. Cell Signal. 2025;131:111715. https://doi.org/10.1016/j.cellsig.2025.111715.
61. Caldeira GL, Ferreira IL, Rego AC. Impaired transcription in Alzheimer's disease: key role in mitochondrial dysfunction and oxidative stress. J Alzheimers Dis. 2013;34(1):115–31. https://doi.org/10.3233/JAD-121444.
62. Bahn G, Park JS, Yun UJ, Lee YJ, Choi Y, Park JS, et al. NRF2/ARE pathway negatively regulates BACE1 expression and ameliorates cognitive deficits in mouse Alzheimer's models. Proc Natl Acad Sci USA. 2019;116(25):12516–23. https://doi.org/10.1073/pnas.1819541116.
63. Duangjan C, Arpawong TE, Spatola BN, Curran SP. Hepatic WDR23 proteostasis mediates insulin homeostasis by regulating insulin-degrading enzyme capacity. Geroscience. 2024;46(5):4461–78. https://doi.org/10.1007/s11357-024-01196-y.
64. Liu L, Martin R, Kohler G, Chan C. Palmitate induces transcriptional regulation of BACE1 and presenilin by STAT3 in neurons mediated by astrocytes. Exp Neurol. 2013;248:482–90. https://doi.org/10.1016/j.expneurol.2013.08.004.
65. Millot P, San C, Bennana E, Porte B, Vignal N, Hugon J, et al. STAT3 inhibition protects against neuroinflammation and BACE1 upregulation induced by systemic inflammation. Immunol Lett. 2020;228:129–34. https://doi.org/10.1016/j.imlet.2020.10.004.
66. Rodriguez-Arellano JJ, Parpura V, Zorec R, Verkhratsky A. Astrocytes in physiological aging and Alzheimer's disease. Neuroscience. 2016;323:170–82.
67. Deng Q, Wu C, Parker E, Liu TC, Duan R, Yang L. Microglia and Astrocytes in Alzheimer's Disease: Significance and Summary of Recent Advances. Aging Disease. 2024;15(4):1537–64. https://doi.org/10.14336/AD.2023.0907.
68. Apodaca LA, Baddour AAD, Garcia C Jr., Alikhani L, Giedzinski E, Ru N, et al. Human neural stem cell-derived extracellular vesicles mitigate hallmarks of Alzheimer's disease. Alzheimers Res Ther. 2021;13(1):57. https://doi.org/10.1186/s13195-021-00791-x.
69. Kaundal RK, Datusalia AK, Sharma SS. Posttranscriptional regulation of Nrf2 through miRNAs and their role in Alzheimer's disease. Pharmacol Res. 2022;175:106018. https://doi.org/10.1016/j.phrs.2021.106018.
70. Martín-Martín Y, Pérez-García A, Torrecilla-Parra M, Fernández-de Frutos M, Pardo-Marqués V, Casarejos MJ, et al. New Insights on the Regulation

of the Insulin-Degrading Enzyme: Role of microRNAs and RBPs. Cells. 2022;11(16):2538. https://doi.org/10.3390/cells11162538.
71. Rong Y, Liu W, Wang J, Fan J, Luo Y, Li L, et al. Neural stem cell-derived small extracellular vesicles attenuate apoptosis and neuroinflammation after traumatic spinal cord injury by activating autophagy. Cell Death Dis. 2019;10(5):340. https://doi.org/10.1038/s41419-019-1571-8.
72. de Munter JPJM, Mey J, Strekalova T, Kramer BW, Wolters EC. Why do anti-inflammatory signals of bone marrow-derived stromal cells improve neurodegenerative conditions where anti-inflammatory drugs fail? J Neural Transm. 2020;127(5):715–27. https://doi.org/10.1007/s00702-020-02173-3.
73. Gao G, Li C, Ma Y, Liang Z, Li Y, Li X, et al. Neural stem cell-derived extracellular vesicles mitigate Alzheimer's disease-like phenotypes in a preclinical mouse model. Signal Transduct Target Therapy. 2023;8(1):228. https://doi.org/10.1038/s41392-023-01436-1.

Publisher's Note